Journal of Materials Chemistry A

ROYAL SOCIETY OF CHEMISTRY

PAPER

View Article Online
View Journal | View Issue

Cite this: J. Mater. Chem. A, 2023, 11, 9691

Water vapour and gas induced phase transformations in an 8-fold interpenetrated diamondoid metal–organic framework†

Aizhamal Subanbekova, ‡[a] Varvara I. Nikolayenko,‡[a] Andrey A. Bezrukov,[a] Debobroto Sensharma,[a] Naveen Kumar,[a] Daniel J. O'Hearn,[a] Volodymyr Bon,[b] Shi-Qiang Wang,[ac] Kyriaki Koupepidou,[a] Shaza Darwish,[a] Stefan Kaskel[b] and Michael J. Zaworotko *[a]

In this work, we report the synthesis, structural characterisation and sorption properties of an 8-fold interpenetrated diamondoid (dia) metal–organic framework (MOF) that is sustained by a new extended linker ligand, [Cd(Imibz)$_2$], **X-dia-2-Cd**, HImibz or 2 = 4-((4-(1*H*-imidazol-1-yl)phenylimino)methyl) benzoic acid. **X-dia-2-Cd** was found to exhibit reversible single-crystal-to-single-crystal (SC–SC) transformations between four distinct phases: an as-synthesised (from *N*,*N*-dimethylformamide) wide-pore phase, **X-dia-2-Cd-α**; a narrow-pore phase, **X-dia-2-Cd-β**, formed upon exposure to water; a narrow-pore phase obtained by activation, **X-dia-2-Cd-γ**; a medium-pore CO_2-loaded phase **X-dia-2-Cd-δ**. While the space group remained constant in the four phases, the cell volumes and calculated void space ranged from 4988.7 Å^3 and 47% (**X-dia-2-Cd-α**), respectively, to 3200.8 Å^3 and 9.1% (**X-dia-2-Cd-γ**), respectively. **X-dia-2-Cd-γ** also exhibited a water vapour-induced structural transformation to the water-loaded **X-dia-2-Cd-β** phase, resulting in an S-shaped sorption isotherm. The inflection point occurred at 18% RH with negligible hysteresis on the desorption profile. Water vapour temperature-humidity swing cycling (60% RH, 300 K to 0% RH, 333 K) indicated hydrolytic stability of **X-dia-2-Cd** and working capacity was retained after 128 cycles of sorbent regeneration. CO_2 (at 195 K) was also observed to induce a structural transformation in **X-dia-2-Cd-γ** and *in situ* PXRD studies at 1 bar of CO_2, 195 K revealed the formation of **X-dia-2-Cd-δ**, which exhibited 31% larger unit cell volume than **X-dia-2-Cd-γ**.

Received 15th March 2023
Accepted 17th April 2023

DOI: 10.1039/d3ta01574b

rsc.li/materials-a

Introduction

Metal–organic frameworks (MOFs) represent a class of porous coordination networks that are of interest thanks in part to their compositional diversity and amenability to fine-tuning of structure and properties by crystal engineering.[1–3] Of the more than 118 000 structures in the MOF subset of the Cambridge Structural Database (CSD),[4–6] the majority are rigid materials that exhibit Type-I gas/vapour sorption isotherms.[7] However, just as molecular materials can undergo gas or vapour induced structural changes,[8] MOFs can also behave as "soft porous crystals".[9] Such flexible metal–organic materials (FMOMs)[10–12] can exhibit stepped or S-shaped isotherms that coincide with a phase transformation that can be regarded as a gate-opening event.[13–15] When FMOMs switch between closed (non-porous or narrow-pore) and open (wide-pore) phases with sharp steps and low hysteresis they offer potential to address the inherent working capacity limitation of rigid porous materials (Fig. 1). These open pore phases may be independent of the identity of the guest species, or may adapt to the dimensions of distinct guests.[16,17] The potential utility of FMOMs for industrial gas storage,[18–20] and, more recently, gas/vapour separations,[21–23] has become apparent, for example Co(bdp),[24] X-dia-1-Ni,[20] UTSA-300 [25] and DUT-8.[26]

With respect to vapour separations, that humanity faces ever-increasing concerns about access to fresh water[27] means that new approaches to atmospheric water harvesting (AWH) are gaining momentum.[28] Currently, there are three primary approaches for AWH: (i) fog collection,[29] (ii) direct cooling of air below its dew point,[30] and (iii) sorbent-assisted (desiccant) capture.[31] While the first two rely on high humidity conditions, only desiccants enable AWH under arid conditions. The study of

[a]Department of Chemical Sciences, Bernal Institute, University of Limerick, Limerick V94 T9PX, Republic of Ireland. E-mail: xtal@ul.ie

[b]Faculty of Chemistry, Technische Universität Dresden, Bergstrasse 66, 01062 Dresden, Germany

[c]Institute of Materials Research and Engineering (IMRE), Agency for Science, Technology and Research (A*STAR), 2 Fusionopolis Way 138634, Singapore

† Electronic supplementary information (ESI) available. CCDC 2240522–2240524. For ESI and crystallographic data in CIF or other electronic format see DOI: https://doi.org/10.1039/d3ta01574b

‡ These authors contributed equally.

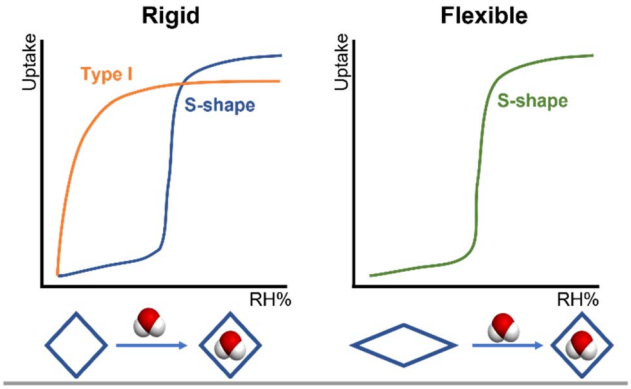

Fig. 1 Schematic of adsorption isotherm types exhibited by rigid MOFs (left) and FMOMs (right). Rigid MOFs typically exhibit type I (orange) or S-shape (blue) isotherms whereas FMOMs tend to exhibit S-shape isotherms (green) resulting from structural transformation(s).

rigid MOFs that exhibit pore-filling at low relative humidity, RH, as alternatives to conventional desiccants such as zeolites and silica gel, is of growing interest in the context of AWH,[32–35] as exemplified by Al-fumarate,[36] MIL-160,[37] MOF-303 [31] and CAU-10-H.[38] FMOMs, which are less studied than rigid MOFs, exhibit a different mechanism, water vapour induced structural transformation(s), *e.g.* JUK-8,[39] [Cu(HQS)(TMBP)],[40] Zn(3-tba)$_2$(H_2O)$_2$,[41] sql-(azpy)(pdia)-Ni[42] and DUT-98.[26] Regardless of the AWH mechanism, key performance parameters include the need for an S-shaped isotherm with an inflection at low RH, negligible hysteresis, low regeneration temperature and hydrolytic/mechanical stability to extended recycling.[43]

MOFs with interpenetrated diamondoid (dia) topology represent one of the most common topologies found in MOFs.[44] Several dia networks have been reported to show stimulus responsive structural transformations induced by various guests.[16,20,39,45–51] In this contribution, we follow on from our previous study on flexible dia topology networks based upon extended ligands or "X-ligands".[20] In our earlier work, switching or S-shaped isotherms enabled by contortions of X-ligands were found to enable high working capacity for natural gas storage in **X-dia-1-Ni**.[18] We herein target 4-((4-(1*H*-imidazol-1-yl) phenylimino)methyl)benzoic acid, HImibz, as an X-ligand (Fig. 2). HImibz, which has not previously been used in coordination chemistry, was of interest to us from crystal engineering (suitability for dia networks), potential properties (torsional flexibility and coordination through an azole moiety)[52] and accessibility (it can be made quantitatively using mechanochemistry)[53] perspectives. Reaction of HImbz with $Cd(NO_3)_2$ indeed afforded an 8-fold interpenetrated dia FMOM, **X-dia-2-Cd**, with composition [Cd(Imibz)$_2$]. We report details of the dynamic behaviour of **X-dia-2-Cd** using single crystal X-ray diffraction (SCXRD), gas and water vapour sorption and *in situ* powder X-ray diffraction (PXRD).

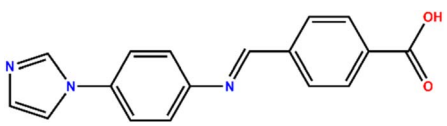

Fig. 2 4-((4-(1*H*-Imidazol-1-yl)phenylimino)methyl)benzoic acid (HImbz), the linker ligand used to synthesise **X-dia-2-Cd**.

Results and discussion

X-ray crystallography and characterisation

HImibz was synthesised by the previously reported procedure, solvent-drop grinding with methanol (MeOH).[53] Single crystals of **X-dia-2-Cd-α** were prepared by solvent layering, whereas bulk samples were synthesised by solvothermal reaction of cadmium nitrate and HImibz in *N*,*N*-dimethylformamide (DMF) (see ESI† for procedure details). SCXRD data revealed that **X-dia-2-Cd-α** (Fig. 3a) had crystallised in the orthorhombic space group *Pnna* with one cadmium cation and one Imibz ligand in the asymmetric unit. Each Cd^{2+} cation coordinates to four carboxylate oxygen atoms from two Imibz linkers and two nitrogen atoms from two additional Imibz linkers, therefore serving as a 4-connected molecular building block (MBB). The pseudotetrahedral MBBs in **X-dia-2-Cd** (Fig. 3b) served as nodes in adamantoid cages (Fig. 3c) that in turn generated a dia topology coordination network with 8-fold interpenetration. A Connolly map[51,52] of the guest accessible volume (1.325 Å probe radius, corresponding to the kinetic diameter of a water molecule) revealed corrugated channels when viewed along the crystallographic *c*-axis accounting for 47% (2344 Å^3) of the unit cell volume (see Table S2† for Connolly surface). Although guest molecules could not be crystallographically resolved, FTIR data indicate the presence of DMF molecules in the pores of **X-dia-2-Cd-α** (Fig. S1 and S2†). Calculated and experimental PXRD patterns of **X-dia-2-Cd-α** are in good agreement, suggesting bulk phase purity (Fig. S3†).

To investigate its hydrolytic stability, **X-dia-2-Cd-α** was immersed in water. Although crystallinity was retained, a different PXRD pattern with prominent peaks undergoing a shift to higher 2θ values was observed, indicating that structural transformation to a smaller unit cell had occurred. In addition to the lateral shifts, there were new PXRD peaks at 8.9°, 17.8° and 21.4° 2θ (Fig. 3d and S3†). The new phase, **X-dia-2-Cd-β**, was also studied by SCXRD. Comparison of the structures of **X-dia-2-Cd-α** and **X-dia-2-Cd-β** collected at 100 K revealed that, although the space group was unchanged, **X-dia-2-Cd-β** had undergone contraction of the *a* and *c*-axes (by 23% and 33%, respectively) and expansion (by 34%) of the *b*-axis. Consequently, the void space had reduced to 15.5% (533 Å^3) and **X-dia-2-Cd-β** may be classified as a narrow-pore phase. Despite the reduction in guest accessible space, two fully occupied and two partially occupied (0.5, 0.5) water molecules were crystallographically located (Fig. 3a). The water molecule contact distances (O1C···O1D = 2.615 Å) are consistent with hydrogen bonding. H-bonding contacts with the host framework were also observed (O1B···O1 = 2.752 Å, O1A···N1A = 3.051 Å). Positional disorder of the aromatic ring and imine bond of the Imibz linker in **X-dia-2-Cd-β** over two general positions (with site occupancies of 0.58 : 0.42, Fig. S4†) is consistent with the disordered water molecules. The experimental PXRD is in good

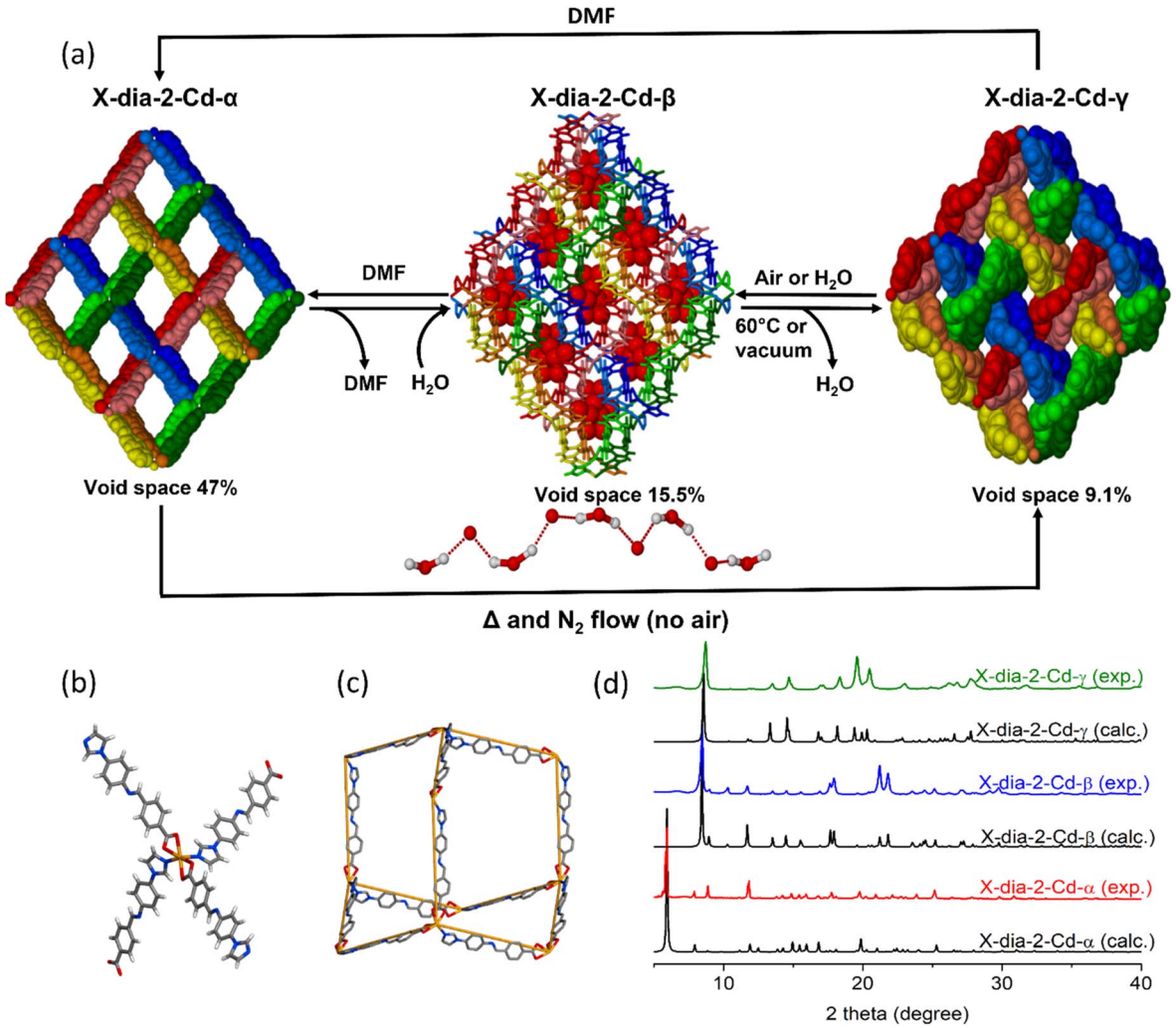

Fig. 3 (a) Crystal packing diagrams illustrating the reversible structural transformations between the three phases of **X-dia-2-Cd**. The water molecules located in the channels of **X-dia-2-Cd-β** are presented in space-fill mode; (b) the tetrahedral MBB present in **X-dia-2-Cd-α** showing the coordination mode for the bi-functional Imibz linker ligand; (c) the adamantoid cage of **X-dia-2-Cd-α**, hydrogen atoms are omitted for clarity; (d) overlaid experimental and calculated PXRD patterns for the three SCXRD characterised phases of **X-dia-2-Cd**.

agreement with that calculated from the SCXRD determined structure of **X-dia-2-Cd-β** (Fig. 3d).

Thermogravimetric analysis (TGA) revealed that **X-dia-2-Cd-α** loses guest molecules below 473 K with no further weight loss until *ca.* 650 K (Fig. S5†). A TGA experiment on **X-dia-2-Cd-β** (Fig. S5†) showed an initial mass loss of 10 wt% below 373 K, corresponding to 4 water molecules per formula unit, and a decomposition temperature of *ca.* 630 K. A series of variable temperature PXRD (VT-PXRD, 298–473 K) experiments under dynamic vacuum and nitrogen flow were performed (see ESI† for details) to study the thermal stability of **X-dia-2-Cd.** Exposure of **X-dia-2-Cd-α** powder to a continuous nitrogen flow for 20 minutes at 298 K triggered a structural transformation accompanied by peak shifts to higher 2θ values (Fig. S6†). Further heating resulted in additional changes, which were complete by 373 K and indicated formation of a new phase, **X-dia-2-Cd-γ**. With additional heating up to 473 K, the PXRD of **X-dia-2-Cd-γ** remained unchanged. Similarly, when a powdered sample of **X-dia-2-Cd-β** was exposed to either vacuum or nitrogen flow (Fig. S7–S9†), conversion to **X-dia-2-Cd-γ** occurred within 20 minutes with no notable change upon heating to 473 K. The phase transformation of **X-dia-2-Cd-β** to **X-dia-2-Cd-γ** was shown to be reversible simply by exposing the **X-dia-2-Cd-γ** to ambient laboratory air for 20 minutes. To determine the crystal structure of **X-dia-2-Cd-γ**, a single crystal of **X-dia-2-Cd-β** was glued to a glass fibre and exposed to a continuous flow of nitrogen at 333 K. Under such conditions, the crystal was exposed to 2.3% RH and SCXRD data were collected (see ESI† for experimental details). Although the crystal structure of **X-dia-2-Cd-γ** retained the same space group as **X-dia-2-Cd-β**, further contraction in the *a* and *b* axes (14% and 4%, respectively), additional expansion (13%) in the *c*-axis, and contraction of the pore volume by 6% (to 9.1%, 291 Å^3) had occurred (Table S1†). The resulting narrow channels exhibit a pore limiting diameter of 2.96 Å and the largest sphere diameter was observed to be 4.13 Å.[54] Although no guest molecules could be

crystallographically located, the residual electron density analysis, as implemented by SQUEEZE,[55] indicated the presence of half a water molecule per asymmetric unit. The PXRD pattern calculated for **X-dia-2-Cd-γ** was found to be in good agreement with the experimental PXRD pattern (Fig. 3d and S3†).

Although the MBB remained unchanged during these transformations, comparison of the SCXRD structures of the three phases revealed that the coordination environment of Cd had undergone considerable change. The pseudotetrahedral 6-coordinated Cd centres exhibited $\tau'_4 = 0.81$ for **X-dia-2-Cd-α**, $\tau'_4 = 0.68$ for **X-dia-2-Cd-β**, and $\tau'_4 = 0.90$ for **X-dia-2-Cd-γ**, indicating that the coordination centre of the guest-free phase is closest to ideal tetrahedral geometry (Table S2†).[56] A CSD survey of Cd pseudotetrahedral coordination environments in the dia TTO subset and 0D CSD subset (search parameters are in SI) revealed that **X-dia-2-Cd-α** is close to the average tetrahedral geometry index among reported materials, while **X-dia-2-Cd-β** and **X-dia-2-Cd-γ** are below and above the mean, respectively (Fig S10 and S11†). Another notable difference was found in the N–Cd–N/C_{COOH}–Cd–C_{COOH} angles; 102°/116°, 112°/140° and 108°/116° for **X-dia-2-Cd-α**, **X-dia-2-Cd-β** and **X-dia-2-Cd-γ**, respectively (Table S3†). Distortion of the Imibz linkers also occurred during the phase transformations, the dihedral angle formed by the benzoate plane and the imidazole plane increasing from 28° in **X-dia-2-Cd-α**, to 63°/67° in **X-dia-2-Cd-β** and 64° in **X-dia-2-Cd-γ**. These in turn resulted in distortions of the adamantanoid cages of the dia networks, with Cd–Cd–Cd angles of 106°/117°, 123°/138°, and 72°/130° for **X-dia-2-Cd-α**, **X-dia-2-Cd-β** and **X-dia-2-Cd-γ**, respectively (Table S3†).

Water vapour sorption

To investigate properties relevant to AWH, Dynamic Vapour Sorption (DVS) data were collected after activating a microcrystalline sample of **X-dia-2-Cd-β** under dry air flow at 333 K, thereby inducing transformation to **X-dia-2-Cd-γ**. The water vapour sorption isotherm was collected at 300 K. Fig. 4a shows that a type F-II[20] reversible isotherm with negligible hysteresis at low RH. After an initial uptake of 2 wt% (*ca.* one water molecule per formula unit, Table S4†), a sudden and pronounced inflection at 18% RH occurred, resulting in adsorption of an additional 13 wt% (total 293 cm^3 cm^{-3}, or *ca.* five water molecules per $Cd(Imibz)_2$ unit at 95% RH). The desorption profile revealed negligible hysteresis during gate-closing and desorption was completed at 17% RH. The isotherms collected at 313 K and 333 K showed a shift of the inflection point to higher RH, 25% and 27% RH respectively (Fig. S12 and S13†). Positions of these inflection points at different temperatures were used to determine enthalpy of phase transition of **X-dia-2-Cd-γ** to **X-dia-2-Cd-β** induced by water sorption. The enthalpy was found to be -53.3 ± 4.4 and 54.6 ± 3.9 kJ mol^{-1} for adsorption and desorption respectively (Fig S14 and S15†), which corresponds well with enthalpy of water vapor sorption for rigid MOMs (Fig S16 and S17†).[31,36–38,57]

To date, the number of FMOMs exhibiting S-shaped water sorption isotherms with inflections below 30% RH (typical ambient RH at arid conditions) remains small. Our review of the literature revealed 32 structures with S-shape water vapour isotherm driven by structural transformation (see Table S6† for details), 13 of which exhibited an inflection point below 30% RH. This review of the literature revealed only two dia networks with S-shape isotherms triggered by a water-induced transformation, JUK-8 [39] and $[Co(HL)_2]\cdot 2H_2O$.[50]

The water vapour sorption kinetics of **X-dia-2-Cd** was evaluated using 0 to 30% RH and 0 to 60% RH humidity swing experiments conducted using a DVS instrument. Kinetics data was fitted with a sorption isotherm-based kinetic model recently published by us[58] (Fig. S18 and 19†). For **X-dia-2-Cd** with an isotherm inflection at 18% RH, the model predicted fast desorption relative to adsorption for 0–30% RH humidity swings and fast adsorption relative to desorption for 0–60% RH humidity swings. The experimentally measured kinetics for a 12.2 mg sample revealed 40 min adsorption *vs.* 30 min desorption and 15 min adsorption *vs.* 30 min desorption respectively, for the two humidity swing conditions.

The recyclability of **X-dia-2-Cd** was evaluated by cycling a sample from 0 to 60% RH for 50 cycles at 300 K (Fig. S20†). Under such conditions, **X-dia-2-Cd** retained its working capacity of 12 wt%. Furthermore, to evaluate the sorbent performance and stability, temperature-humidity swing cycling was performed (300 K, 60% RH to 333 K, 0% RH). Fig. 4b reveals that **X-dia-2-Cd** maintained working capacity of 12 wt% for 128 cycles.

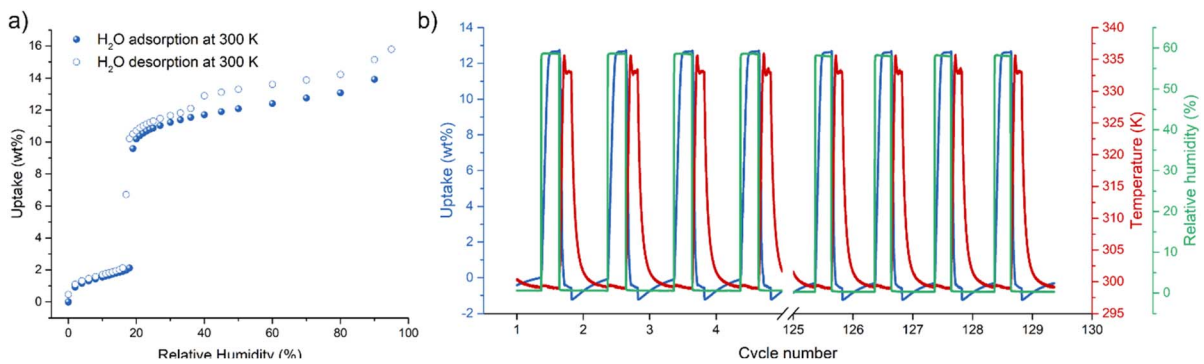

Fig. 4 (a) Water vapour sorption isotherms for X-dia-2-Cd-γ measured at 300 K; (b) cycling experiment for X-dia-2-Cd-γ under temperature-humidity swing conditions (300 K, 60% RH to 333 K, 0% RH).

To the best of our knowledge **X-dia-2-Cd** is only the second FMOM, after [Cu(HQS)(TMBP)],[40] confirmed to exhibit hydrolytic stability over 100+ temperature-humidity swing cycles of water vapour sorption. Whereas rigid MOFs are being explored as candidates for AWH, flexible MOFs are typically considered to be unsuitable, mainly because of concerns over kinetics and mechanical stress. To the best of our knowledge, **X-dia-2-Cd** is the first flexible MOF that meets all 4 of the main criteria for utility in AWH (Table S6†): an S-shape isotherm with inflection point below 30% RH; negligible hysteresis (<5 RH%); mild regeneration temperature (333 K); hydrolytic stability during temperature-humidity swing cycles for 100+ cycles.

Gas sorption and *in situ* coincident PXRD

The observed structural flexibility of **X-dia-2-Cd** prompted us to also investigate its gas sorption properties. A bulk sample of **X-dia-2-Cd-β** was heated at 373 K under vacuum to afford **X-dia-2-Cd-γ**; gas sorption isotherms were recorded for N_2 at 77 K and for CO_2 and C_2H_2 at 195 K (Fig. 5). At 77 K, **X-dia-2-Cd** did not exhibit N_2 uptake, which agrees with the calculated pore limiting diameter of **X-dia-2-Cd-γ** (2.96 Å) and the kinetic diameter of N_2 (3.64 Å).[59] The CO_2 and C_2H_2 gas sorption isotherms collected at 195 K revealed stepped type F-II behaviour.[20] For CO_2, initial loading of *ca.* 25 $cm^3\ g^{-1}$ of CO_2 was followed by a sharp inflection at 0.06 bar, after which an additional 65 cm^3 g was adsorbed. To gain further insight, we performed *in situ* PXRD during CO_2 sorption at 195 K (Fig. 6 and S21†). At 0.3041 bar, **X-dia-2-Cd-γ** adsorbed 25 $cm^3\ g^{-1}$ of CO_2 without any significant structural changes, consistent with retention of **X-dia-2-Cd-γ** at these conditions (Fig. S21†). As CO_2 pressure increased, the formation of a new CO_2 loaded phase, **X-dia-2-Cd-δ**, occurred, with a unit cell volume of 4627.17, 31% larger than that of **X-dia-2-Cd-γ** (Fig. S22†). Upon desorption, the material reverted to **X-dia-2-Cd-γ**. A similar isotherm shape indicating a phase transition in **X-dia-2-Cd** upon CO_2 sorption was obtained during high pressure gravimetric CO_2 experiments at 273 K (Fig. S23†).

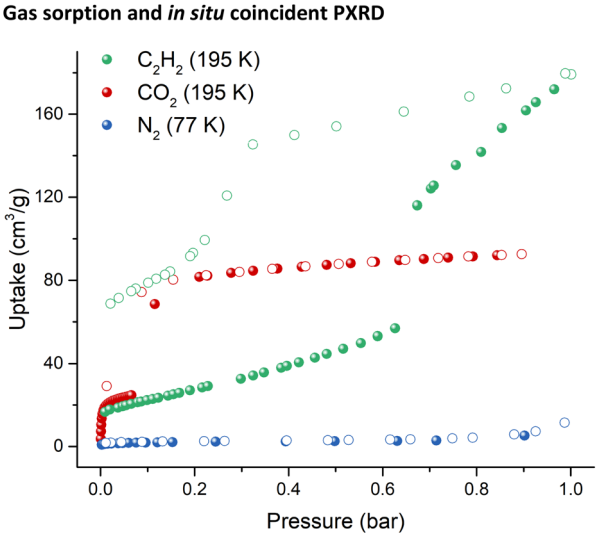

Fig. 5 Gas sorption on **X-dia-2-Cd-γ**: C_2H_2 at 195 K (green), CO_2 at 195 K (red) and N_2 at 77 K (blue).

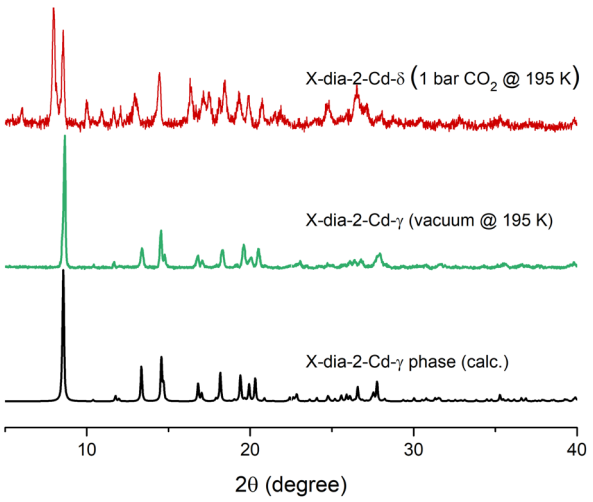

Fig. 6 *In situ* PXRD measured during adsorption of CO_2 on **X-dia-2-Cd-γ** at 195 K.

Gas sorption experiments at 273 K and 298 K were performed for CO_2, C_2 gases (C_2H_2, C_2H_4, and C_2H_6) and C_3 gases (C_3H_4, C_3H_6, C_3H_8) (Fig. S24–S27†). In almost all cases, **X-dia-2-Cd** showed a type I gas sorption isotherm below 1 bar, except in the cases of C_2H_6 and C_3H_8, for which stepped isotherms were observed. 298 K sorption data on **X-dia-2-Cd** revealed higher uptake at 1 bar for C_2H_2 (30 $cm^3\ g^{-1}$) than for CO_2 (10 $cm^3\ g^{-1}$). A dynamic column breakthrough experiment confirmed separation of C_2H_2 from a C_2H_2/CO_2 1 : 1 v:v mixture by **X-dia-2-Cd** (Fig. S28†), although the separation factor is lower than that predicted by IAST (Fig. S29,† $\alpha_{AC} = 2.32$ from breakthrough experiment *vs.* 174 from IAST calculation). We attribute this performance to the structural flexibility of **X-dia-2-Cd** and co-adsorption in the more open phase(s).[60]

General discussion of why dia networks are common and attractive for study including CSD data mining

Diamondoid networks seem well-suited for crystal engineering of new FMOMs because of the factors that are likely to facilitate structural flexibility, *e.g.* low coordination number and interpenetration, which can stabilise large pores. From the perspective of crystal engineering of dia networks, our analysis of TOPOS TTO∩CSD[4,61] databases (Fig. S30, see ESI† for details) revealed that, in the case of single-linker dia networks, in addition to bi-functional N-donor + carboxylate linkers such as HImibz (213 structures), prospective families include dia networks based on N-donor linkers (209 structures), and dicarboxylate linkers (167 structures) (Fig. S30†). A mixed-linker crystal engineering approach was recently proven successful for the development of sorbents with sql network topologies,[62] and appears promising for dia type networks as well, as there are 566 mixed-linker networks containing both N-donor (*e.g.* 4,4′-bipyridine) and dicarboxylate (*e.g.* 1,4-benzenedicarboxylate) linkers (Fig. S30†).[16,45,61] Interpenetration is a common

characteristic of dia networks due to their topological features and their relatively large cavities, pores and channels. While porous non-interpenetrated networks tend to be structurally unstable, interpenetration of dia nets decreases the free volume and increases the density of the network, sometimes eliminating porosity if the degree of interpenetration is high enough. Our analysis of network interpenetration in dia networks using TOPOS[62] revealed that MOFs based on mixed-linkers or bifunctional (N-donor + carboxylate) linkers are more likely to interpenetrate, while MOF based on other linkers tend towards generating non-interpenetrated networks (Fig. S31–S35†). We also found that most mixed-linker dia nets exhibit little or no void space (Fig. S31†).

Despite the amenability of dia networks to crystal engineering discussed above, our analysis of dia MOFs in the (CSD database)∩(TTO database) shows that, out of the 1973 reported structures, only 116 (<6%) were subjected to sorption studies. Whilst the majority of the dia nets studied for sorption are rigid compounds with Type I isotherms, 29 demonstrated structural flexibility during gas/vapour sorption (Table S9†). 11 of these flexible structures are based on mixed linkers, the remainder are single-linker structures, 10 being bifunctional. This database and literature search indicates that dia networks remain relatively understudied and suggests that more sorption studies are needed in order to properly evaluate their potential for gas and vapour-related applications.

Conclusions

We herein report the new MOF **X-dia-2-Cd**, that, despite a high level of interpenetration (8-fold), underwent reversible transformations with significant change of accessible void space between the as-synthesised phase (47%), water loaded phase (15.5%) and activated phase (9.1%). Despite this high level of structural flexibility, **X-dia-2-Cd** retained crystallinity for all phases, which were characterised by XRD studies in order to obtain structural insight into the host–guest interactions, ligand contortions and coordination environments that enabled this structural flexibility.

Perhaps the most salient aspect of this work concerns what it says about the potential utility of FMOMs. In particular, we provide a proof-of-concept that structurally flexible water sorbents can meet the key performance criteria for a water sorbent to become a viable candidate for AWH: S-shape isotherm with an inflection at low RH; negligible hysteresis; low temperature of regeneration; hydrolytic stability over extended cycling. We consider it likely that the crystal engineering approach outlined herein would be feasible to develop families of related structurally flexible materials improve working capacity and tune threshold RH for other water vapour sorption applications, studies concerning which are currently underway.

Author contributions

M. J. Z., A. S. and V. I. N. conceived the original idea and A. A. B. performed the database searches. A. S. and V. I. N. performed the synthesis, structure and property analysis, SCXRD experiments and wrote the manuscript. A. A. B., S. D. and D. J. O. performed water vapour sorption experiments. D. S., K. K., and S.-Q. W. performed gas sorption experiments. A. S., D. J. O. and D. S. performed PXRD experiments. A. S. and N. K performed VT-PXRD experiments. V. B. and S. K. performed *in situ* PXRD experiments. A. S. and V. I. N. contributed equally. All authors contributed to manuscript writing.

Conflicts of interest

There are no conflicts to declare.

Acknowledgements

M. J. Z. gratefully acknowledges the support from the Irish Research Council (IRCLA/2019/167), the European Research Council (ADG 885695) and Science Foundation Ireland (16/IA/4624). S. K. acknowledges support from the European Research Council (DYNADIFF No. 966772). We would also like to thank Diamond Light Source for access to beamline I11 (CY30456-1), especially Dr Stephen Thompson, Dr Lucy Saunders and Dr Sarah Day. The authors would like to thank their colleague Dr Benjamin H. Wilson for his assistance at Diamond Light Source and Dr Sergey Beloshapkin for his kind help with the VT PXRD experiment.

References

1 B. Moulton and M. J. Zaworotko, From Molecules to Crystal Engineering: Supramolecular Isomerism and Polymorphism in Network Solids, *Chem. Rev.*, 2001, **101**, 1629–1658.
2 S. Kitagawa, R. Kitaura and S. I. Noro, Functional Porous Coordination Polymers, *Angew. Chem., Int. Ed.*, 2004, **43**, 2334–2375.
3 H. Li, M. Eddaoudi, M. O'Keeffe and O. M. Yaghi, Design and synthesis of an exceptionally stable and highly porous metal-organic framework, *Nature*, 1999, **402**, 276–279.
4 P. Z. Moghadam, A. Li, S. B. Wiggin, A. Tao, A. G. P. Maloney, P. A. Wood, S. C. Ward and D. Fairen-Jimenez, Development of a Cambridge Structural Database Subset: A Collection of Metal–Organic Frameworks for Past, Present, and Future, *Chem. Mater.*, 2017, **29**, 2618–2625.
5 C. R. Groom, I. J. Bruno, M. P. Lightfoot and S. C. Ward, The Cambridge Structural Database, *Acta Crystallogr., Sect. B: Struct. Sci., Cryst. Eng. Mater.*, 2016, **72**, 171–179.
6 P. Z. Moghadam, A. Li, X. W. Liu, R. Bueno-Perez, S. D. Wang, S. B. Wiggin, P. A. Wood and D. Fairen-Jimenez, Targeted classification of metal–organic frameworks in the Cambridge structural database (CSD), *Chem. Sci.*, 2020, **11**, 8373–8387.
7 M. Thommes, K. Kaneko, A. V. Neimark, J. P. Olivier, F. Rodriguez-Reinoso, J. Rouquerol and K. S. W. Sing, Physisorption of gases, with special reference to the evaluation of surface area and pore size distribution (IUPAC Technical Report), *Pure Appl. Chem.*, 2015, **87**, 1051–1069.

8 S. A. Allison and R. M. Barrer, Sorption in the β-phases of transition metal(II) tetra-(4-methylpyridine) thiocyanates and related compounds, *J. Chem. Soc. A*, 1969, 1717–1723.
9 S. Horike, S. Shimomura and S. Kitagawa, Soft porous crystals, *Nat. Chem.*, 2009, **1**, 695–704.
10 Z. Chang, D.-H. Yang, J. Xu, T.-L. Hu and X.-H. Bu, Flexible Metal–Organic Frameworks: Recent Advances and Potential Applications, *Adv. Mater.*, 2015, **27**, 5432–5441.
11 G. Férey and C. Serre, Large breathing effects in three-dimensional porous hybrid matter: facts, analyses, rules and consequences, *Chem. Soc. Rev.*, 2009, **38**, 1380–1399.
12 L. Sarkisov, R. L. Martin, M. Haranczyk and B. Smit, On the Flexibility of Metal–Organic Frameworks, *J. Am. Chem. Soc.*, 2014, **136**, 2228–2231.
13 S. Q. Wang, S. Mukherjee and M. J. Zaworotko, Spiers Memorial Lecture: Coordination networks that switch between nonporous and porous structures: An emerging class of soft porous crystals, *Faraday Discuss.*, 2021, **231**, 9–50.
14 A. Schneemann, V. Bon, I. Schwedler, I. Senkovska, S. Kaskel and R. A. Fischer, Flexible metal–organic frameworks, *Chem. Soc. Rev.*, 2014, **43**, 6062–6096.
15 S. Krause, N. Hosono and S. Kitagawa, Chemistry of Soft Porous Crystals: Structural Dynamics and Gas Adsorption Properties, *Angew. Chem., Int. Ed.*, 2020, **59**, 15325–15341.
16 E. J. Carrington, C. A. McAnally, A. J. Fletcher, S. P. Thompson, M. Warren and L. Brammer, Solvent-switchable continuous-breathing behaviour in a diamondoid metal–organic framework and its influence on CO_2 versus CH_4 selectivity, *Nat. Chem.*, 2017, **9**, 882–889.
17 C. Serre, C. Mellot-Draznieks, S. Surblé, N. Audebrand, Y. Filinchuk and G. Férey, Role of Solvent-Host Interactions That Lead to Very Large Swelling of Hybrid Frameworks, *Science*, 2007, **315**, 1828–1831.
18 S.-Q. Wang, S. Darwish, X.-Q. Meng, Z. Chang, X.-H. Bu and M. J. Zaworotko, Acetylene storage performance of [Ni(4,4′-bipyridine)2(NCS)2]n, a switching square lattice coordination network, *Chem. Commun.*, 2022, **58**, 1534–1537.
19 C. M. Simon, J. Kim, D. A. Gomez-Gualdron, J. S. Camp, Y. G. Chung, R. L. Martin, R. Mercado, M. W. Deem, D. Gunter, M. Haranczyk, D. S. Sholl, R. Q. Snurr and B. Smit, The materials genome in action: identifying the performance limits for methane storage, *Energy Environ. Sci.*, 2015, **8**, 1190–1199.
20 Q. Y. Yang, P. Lama, S. Sen, M. Lusi, K. J. Chen, W. Y. Gao, M. Shivanna, T. Pham, N. Hosono, S. Kusaka, J. J. Perry, S. Ma, B. Space, L. J. Barbour, S. Kitagawa and M. J. Zaworotko, Reversible Switching between Highly Porous and Nonporous Phases of an Interpenetrated Diamondoid Coordination Network That Exhibits Gate-Opening at Methane Storage Pressures, *Angew. Chem., Int. Ed.*, 2018, **57**, 5684–5689.
21 S. Mukherjee, D. Sensharma, K.-J. Chen and M. J. Zaworotko, Crystal engineering of porous coordination networks to enable separation of C2 hydrocarbons, *Chem. Commun.*, 2020, **56**, 10419–10441.
22 Q. Qian, P. A. Asinger, M. J. Lee, G. Han, K. Mizrahi Rodriguez, S. Lin, F. M. Benedetti, A. X. Wu, W. S. Chi and Z. P. Smith, MOF-Based Membranes for Gas Separations, *Chem. Rev.*, 2020, **120**, 8161–8266.
23 M. Shah, M. C. McCarthy, S. Sachdeva, A. K. Lee and H.-K. Jeong, Current Status of Metal–Organic Framework Membranes for Gas Separations: Promises and Challenges, *Ind. Eng. Chem. Res.*, 2012, **51**, 2179–2199.
24 J. A. Mason, J. Oktawiec, M. K. Taylor, M. R. Hudson, J. Rodriguez, J. E. Bachman, M. I. Gonzalez, A. Cervellino, A. Guagliardi, C. M. Brown, P. L. Llewellyn, N. Masciocchi and J. R. Long, Methane storage in flexible metal–organic frameworks with intrinsic thermal management, *Nature*, 2015, **527**, 357–361.
25 R.-B. Lin, L. Li, H. Wu, H. Arman, B. Li, R.-G. Lin, W. Zhou and B. Chen, Optimized Separation of Acetylene from Carbon Dioxide and Ethylene in a Microporous Material, *J. Am. Chem. Soc.*, 2017, **139**, 8022–8028.
26 S. Krause, V. Bon, H. Du, R. E. Dunin-Borkowski, U. Stoeck, I. Senkovska and S. Kaskel, The impact of crystal size and temperature on the adsorption-induced flexibility of the Zr-based metal–organic framework DUT-98, *Beilstein J. Nanotechnol.*, 2019, **10**, 1737–1744.
27 *W. U. W. W. A. Programme and the United Nations World Water Development Report 2019: Leaving No One behind*, Report 978-92-3-100309-7, UNESCO, 2019.
28 J. Lord, A. Thomas, N. Treat, M. Forkin, R. Bain, P. Dulac, C. H. Behroozi, T. Mamutov, J. Fongheiser, N. Kobilansky, S. Washburn, C. Truesdell, C. Lee and P. H. Schmaelzle, Global potential for harvesting drinking water from air using solar energy, *Nature*, 2021, **598**, 611–617.
29 R. S. Schemenauer and P. Cereceda, A Proposed Standard Fog Collector for Use in High-Elevation Regions, *J. Appl. Meteorol. Climatol.*, 1994, **33**, 1313–1322.
30 R. V. Wahlgren, Atmospheric water vapour processor designs for potable water production: a review, *Water Res.*, 2001, **35**, 1–22.
31 N. Hanikel, M. S. Prévot, F. Fathieh, E. A. Kapustin, H. Lyu, H. Wang, N. J. Diercks, T. G. Glover and O. M. Yaghi, Rapid Cycling and Exceptional Yield in a Metal-Organic Framework Water Harvester, *ACS Cent. Sci.*, 2019, **5**, 1699–1706.
32 H. Kim, S. Yang, S. R. Rao, S. Narayanan, E. A. Kapustin, H. Furukawa, A. S. Umans, O. M. Yaghi and E. N. Wang, Water harvesting from air with metal-organic frameworks powered by natural sunlight, *Science*, 2017, **356**, 430–434.
33 Y. K. Seo, J. W. Yoon, J. S. Lee, Y. K. Hwang, C. H. Jun, J. S. Chang, S. Wuttke, P. Bazin, A. Vimont, M. Daturi, S. Bourrelly, P. L. Llewellyn, P. Horcajada, C. Serre and G. Férey, Energy-Efficient Dehumidification over Hierachically Porous Metal–Organic Frameworks as Advanced Water Adsorbents, *Adv. Mater.*, 2012, **24**, 806–810.
34 A. J. Rieth, S. Yang, E. N. Wang and M. Dincă, Record Atmospheric Fresh Water Capture and Heat Transfer with a Material Operating at the Water Uptake Reversibility Limit, *ACS Cent. Sci.*, 2017, **3**, 668–672.
35 S. M. Towsif Abtab, D. Alezi, P. M. Bhatt, A. Shkurenko, Y. Belmabkhout, H. Aggarwal, Ł. J. Weseliński, N. Alsadun,

U. Samin, M. N. Hedhili and M. Eddaoudi, Reticular Chemistry in Action: A Hydrolytically Stable MOF Capturing Twice Its Weight in Adsorbed Water, *Chem*, 2018, **4**, 94–105.

36 F. Jeremias, D. Fröhlich, C. Janiak and S. K. Henninger, Advancement of sorption-based heat transformation by a metal coating of highly-stable, hydrophilic aluminium fumarate MOF, *RSC Adv.*, 2014, **4**, 24073–24082.

37 A. Cadiau, J. S. Lee, D. Borges, P. Fabry, T. Devic, M. T. Wharmby, C. Martineau, D. Foucher, F. Taulelle, C.-H. Jun, Y. K. Hwang, N. Stock, M. F. De Lange, F. Kapteijn, J. Gascon, G. Maurin, J.-S. Chang, C. Serre, A. Cadiau, P. Fabry, T. Devic, C. Martineau, D. Foucher, F. Taulelle, C. Serre, J. S. Lee, Y. K. Hwang, J. S. Chang, C. H. Jun, D. Damasceno-Borges, G. Maurin, M. F. De Lange, F. Kapteijn and J. Gascon, Design of Hydrophilic Metal Organic Framework Water Adsorbents for Heat Reallocation, *Adv. Mater.*, 2015, **27**, 4775–4780.

38 D. Fröhlich, E. Pantatosaki, P. D. Kolokathis, K. Markey, H. Reinsch, M. Baumgartner, M. A. Van Der Veen, D. E. De Vos, N. Stock, G. K. Papadopoulos, S. K. Henninger and C. Janiak, Water adsorption behaviour of CAU-10-H: a thorough investigation of its structure–property relationships, *J. Mater. Chem. A*, 2016, **4**, 11859–11869.

39 K. Roztocki, F. Formalik, A. Krawczuk, I. Senkovska, B. Kuchta, S. Kaskel and D. Matoga, Collective Breathing in an Eightfold Interpenetrated Metal–Organic Framework: From Mechanistic Understanding towards Threshold Sensing Architectures, *Angew. Chem., Int. Ed.*, 2020, **59**, 4491–4497.

40 M. Shivanna, A. A. Bezrukov, V. Gascón-Pérez, K. I. Otake, S. Sanda, D. J. O'Hearn, Q. Y. Yang, S. Kitagawa and M. J. Zaworotko, Flexible Coordination Network Exhibiting Water Vapor-Induced Reversible Switching between Closed and Open Phases, *ACS Appl. Mater. Interfaces*, 2022, **14**, 39560–39566.

41 M. Deng, S. Mukherjee, Y.-J. Liang, X.-D. Fang, A.-X. Zhu and M. Zaworotko, Water vapour induced reversible switching between a 1-D coordination polymer and a 0-D aqua complex, *Chem. Commun.*, 2022, **58**, 8218–8221.

42 X. Li, D. Sensharma, V. I. Nikolayenko, S. Darwish, A. A. Bezrukov, N. Kumar, W. Liu, X.-J. Kong, Z. Zhang and M. J. Zaworotko, Structural Phase Transformations Induced by Guest Molecules in a Nickel-Based 2D Square Lattice Coordination Network, *Chem. Mater.*, 2023, **35**, 783–791.

43 X. Liu, X. Wang and F. Kapteijn, Water and Metal-Organic Frameworks: From Interaction toward Utilization, *Chem. Rev.*, 2020, **120**, 8303–8377.

44 T. G. Mitina and V. A. Blatov, Topology of 2-Periodic Coordination Networks: Toward Expert Systems in Crystal Design, *Cryst. Growth Des.*, 2013, **18**, 6.

45 J. H. Park, W. R. Lee, Y. Kim, H. J. Lee, D. W. Ryu, W. J. Phang and C. S. Hong, Interpenetration control, sorption behavior, and framework flexibility in Zn(II) metal-organic frameworks, *Cryst. Growth Des.*, 2014, **14**, 699–704.

46 C. T. He, P. Q. Liao, D. D. Zhou, B. Y. Wang, W. X. Zhang, J. P. Zhang and X. M. Chen, Visualizing the distinctly different crystal-to-crystal structural dynamism and sorption behavior of interpenetration-direction isomeric coordination networks, *Chem. Sci.*, 2014, **5**, 4755–4762.

47 S. S. Chen, Q. Liu, Y. Zhao, R. Qiao, L. Q. Sheng, Z. D. Liu, S. Yang and C. F. Song, New metal-organic frameworks constructed from the 4-imidazole-carboxylate ligand: Structural diversities, luminescence, and gas adsorption properties, *Cryst. Growth Des.*, 2014, **14**, 3727–3741.

48 B. Zhou, T. Zeng, Z.-L. Shi, G. Zhang, S. Horike, Y.-B. Zhang and B. Zhou, An Allosteric Metal–Organic Framework That Exhibits Multiple Pore Configurations for the Optimization of Hydrocarbon Separation, *Chem.–Asian J.*, 2019, **14**, 3552–3556.

49 Z. Cao, L. Chen, S. Li, M. Yu, Z. Li, K. Zhou, C. P. Liu, F. Jiang and M. Hong, A Flexible Two-Fold Interpenetrated Indium MOF Exhibiting Dynamic Response to Gas Adsorption and High-Sensitivity Detection of Nitroaromatic Explosives, *Chem.–Asian J.*, 2019, **14**, 3597–3602.

50 S.-S. Chen, G.-C. Lv, J. Fan, T.-a. Okamura, M. Chen and W.-Y. Sun, Entangled coordination frameworks with 1,4-Di(1 H -imidazole-4-yl)benzene, *Cryst. Growth Des.*, 2011, **11**, 1082–1090.

51 J. Lopex-Cabrelles, J. Romero, G. Abella, n. Gime, M. Palomino, S. Valencia, F. Rey, G. Mínguez Espallargas and T. Jose, Solvent-Free Synthesis of ZIFs: A Route toward the Elusive Fe(II) Analogue of ZIF-8, *J. Am. Chem. Soc.*, 2019, **17**, 7173–7180.

52 S. B. Copp, S. Subramanian and M. J. Zaworotko, Supramolecular chemistry of manganese complex [Mn(CO)3(.mu.3-OH)]4: assembly of a cubic hydrogen-bonded diamondoid network with 1,2-diaminoethane, *J. Am. Chem. Soc.*, 1992, **114**, 8719–8720.

53 R. Sanii, A. Bajpai, E. Patyk-Kaźmierczak and M. J. Zaworotko, High Yield, Low-Waste Synthesis of a Family of Pyridyl and Imidazolyl-Substituted Schiff Base Linker Ligands, *ACS Sustainable Chem. Eng.*, 2018, **6**, 14589–14598.

54 T. F. Willems, C. H. Rycroft, M. Kazi, J. C. Meza and M. Haranczyk, Algorithms and tools for high-throughput geometry-based analysis of crystalline porous materials, *Microporous Mesoporous Mater.*, 2012, **149**, 134–141.

55 A. L. Spek, PLATON SQUEEZE: a tool for the calculation of the disordered solvent contribution to the calculated structure factors, *Acta Crystallogr., Sect. C: Struct. Chem.*, 2015, **71**, 9–18.

56 A. Okuniewski, D. Rosiak, J. Chojnacki and B. Becker, Coordination polymers and molecular structures among complexes of mercury(II) halides with selected 1-benzoylthioureas, *Polyhedron*, 2015, **90**, 47–57.

57 H. Furukawa, F. Gándara, Y. B. Zhang, J. Jiang, W. L. Queen, M. R. Hudson and O. M. Yaghi, Water adsorption in porous metal-organic frameworks and related materials, *J. Am. Chem. Soc.*, 2014, **136**, 4369–4381.

58 A. A. Bezrukov, D. J. O'Hearn, V. Gascón-Pérez, S. Darwish, A. Kumar, S. Sanda, N. Kumar, K. Francis and

M. J. Zaworotko, Metal-organic frameworks as regeneration optimized sorbents for atmospheric water harvesting, *Cell Rep. Phys. Sci.*, 2023, 101252.

59 D. W. Breck, Crystalline molecular sieves, *J. Chem. Educ.*, 1964, **41**, 678–689.

60 G. Fraux, A. Boutin, A. H. Fuchs and F.-X. Coudert, On the use of the IAST method for gas separation studies in porous materials with gate-opening behavior, *Adsorption*, 2018, **24**, 233–241.

61 D.-Y. Ma, Z. Li, J.-X. Xiao, R. Deng, P.-F. Lin, R.-Q. Chen, Y.-Q. Liang, H.-F. Guo, B. Liu and J.-Q. Liu, Hydrostable and Nitryl/Methyl-Functionalized Metal–Organic Framework for Drug Delivery and Highly Selective CO_2 Adsorption, *Inorg. Chem.*, 2015, **54**, 6719–6726.

62 N. Kumar, S. Q. Wang, S. Mukherjee, A. A. Bezrukov, E. Patyk-Kaźmierczak, D. O'Nolan, A. Kumar, M. H. Yu, Z. Chang, X. H. Bu and M. J. Zaworotko, Crystal engineering of a rectangular sql coordination network to enable xylenes selectivity over ethylbenzene, *Chem. Sci.*, 2020, **11**, 6889–6895.